

Galaxy merging, the Fundamental Plane of elliptical galaxies, and the $M_{\text{BH}}\text{-}\sigma_0$ relation

C. Nipoti,¹ P. Londrillo² and L. Ciotti^{1,3}

¹*Dipartimento di Astronomia, Università di Bologna, via Ranzani 1, 40127 Bologna, Italy*

²*INAF - Osservatorio Astronomico di Bologna, via Ranzani 1, 40127 Bologna, Italy*

³*Scuola Normale Superiore, Piazza dei Cavalieri 7, 56126 Pisa, Italy*

Accepted version 19/02/2003, submitted in original form 16/09/2002

ABSTRACT

We explore the effects of *dissipationless* merging on the Fundamental Plane of elliptical galaxies by using a N-body code based on a new, high performance numerical scheme (Dehnen 2002). We investigate the two extreme cases of galaxy growth by *equal mass merging* and *accretion* of small stellar systems; in a subset of simulations we also consider the presence of dark matter halos around the merging galaxies. Curiously, we found that the Fundamental Plane is preserved by major merging, while in the accretion scenario its edge–on thickness is only marginally reproduced, with substantial thickening in the case of merging with low angular momentum. We also found that both the Faber–Jackson and Kormendy relations are *not* reproduced by the simulations, in accordance with the results of a preliminary analysis based on a simple application of the virial theorem. Finally, we discuss the implications of our results for the origin of the $M_{\text{BH}}\text{-}\sigma_0$ and Magorrian relations. We found that dissipationless merging is unable to reproduce the $M_{\text{BH}}\text{-}\sigma_0$ relation, if the black hole masses add linearly (while the Magorrian relation is nicely reproduced); on the contrary a black hole merging with substantial emission of gravitational waves reproduces the $M_{\text{BH}}\text{-}\sigma_0$ relation but fails at reproducing the Magorrian relation. We argue that our results strongly point towards a major role of *dissipation* in the formation of early–type galaxies and in the growth of their central supermassive black holes, thus supporting the idea of a link between galaxy formation and QSO activity.

Key words:

galaxies: elliptical and lenticular, cD – galaxies: formation – galaxies: kinematics and dynamics – galaxies: fundamental parameters – black hole physics

1 INTRODUCTION

Two distinct scenarios have been proposed to describe the formation of elliptical galaxies (Es): roughly speaking, according to the *monolithic scenario* Es form at high redshift in dissipative collapses (see, e.g., Eggen, Lynden-Bell & Sandage 1962, Larson 1975), while in the *hierarchical merging scenario* spheroidal systems are the end–products of several merging processes of smaller galaxies, the last major merger taking place in relatively recent times, i.e. at $z \lesssim 1$ (see, e.g., White & Rees 1978, Kauffmann 1996, Cole et al. 2000). In particular, this second picture is supported by some observational data suggesting that a fraction of red galaxies in clusters at intermediate redshift are undergoing merging processes: these galaxies could be the progenitors of present–day early–type galaxies (van Dokkum et al. 1999).

In any case, it is well known that Es satisfy many scaling

relations (more or less tight) that must be accounted for by any proposed formation scenario: for example the Faber–Jackson relation (hereafter FJ, Faber & Jackson 1976), the Kormendy relation (Kormendy 1977), the $\text{Mg}_2\text{-}\sigma_0$ relation (see, e.g., Burstein et al. 1988, Bender, Burstein & Faber 1993) the color–magnitude relation (Bower, Lucey & Ellis 1992), and the very tight Fundamental Plane (hereafter FP; Djorgovski & Davis 1987, Dressler et al. 1987). In addition, it is now widely accepted that central supermassive black holes (hereafter BHs) are a common characteristic of spheroidal stellar systems (see, e.g., Kormendy & Richstone 1995, van der Marel 1999, de Zeeuw 2001); it has also been found that their mass (M_{BH}) is linearly proportional to the mass of the host spheroid (Magorrian et al. 1998), and it is even more correlated with the spheroid central stellar velocity dispersion (Gebhardt et al. 2000, Ferrarese & Merritt 2000). Due to their relevance in this work, here we briefly review

the main properties of the FP, FJ, Kormendy and $M_{\text{BH}}-\sigma_0$ relations.

The FP of Es is a scaling relation between three of their basic *observational* properties, namely the circularized effective radius $\langle R \rangle_e \equiv \sqrt{a_e b_e}$ (where a_e and b_e are the major and minor semi-axis of the effective isophotal ellipse), the central velocity dispersion σ_0 , and the mean effective surface brightness $\langle I \rangle_e \equiv L_B / 2\pi \langle R \rangle_e^2$ (where L_B is the luminosity of the galaxy, for example in the Johnson B-band). A parameterization of the FP, that we adopt in this paper, has been introduced by Bender, Burstein & Faber (1992, hereafter BBF), by defining the three variables

$$k_1 \equiv \frac{\log \sigma_0^2 + \log \langle R \rangle_e}{\sqrt{2}}, \quad (1)$$

$$k_2 \equiv \frac{\log \sigma_0^2 + 2 \log \langle I \rangle_e - \log \langle R \rangle_e}{\sqrt{6}}, \quad (2)$$

$$k_3 \equiv \frac{\log \sigma_0^2 - \log \langle I \rangle_e - \log \langle R \rangle_e}{\sqrt{3}}. \quad (3)$$

In particular, when projected on the (k_1, k_3) plane, the FP is seen almost edge-on and it is considerably thin, while the distribution of galaxies in the (k_1, k_2) plane is broader. For example, Virgo ellipticals studied by BBF are distributed on the (k_1, k_3) plane according to the best-fit relation

$$k_3 = 0.15k_1 + 0.36, \quad (4)$$

(when adopting respectively, kpc, km s^{-1} and $L_{B\odot} \text{ pc}^{-2}$ as length, velocity and surface brightness units), with a very small 1- σ dispersion of $\text{rms}(k_3) \simeq 0.05$ over the whole range spanned by the data, $2.6 \lesssim k_1 \lesssim 4.6$ ($0.75 \lesssim k_3 \lesssim 1.05$). This translates in a scatter of $\simeq 15\%$ in $\langle R \rangle_e$ for fixed L_B and σ_0 . The slope and the scatter of equation (4) are usually called “tilt” and “thickness” of the FP, respectively. By combining equations (1) and (3) with equation (4) the FP relation is obtained in terms of the observables, and is in good agreement with the FP derived (in the same photometric band and for a much larger galaxy sample) by Jørgensen, Franx & Kjærgaard (1996)*.

Strictly related to the FP are the less tight FJ and Kormendy relations. These scaling relations have been often interpreted just as projections of the FP with no additional information, and, for this reason, their constraining power on galaxy formation scenarios has been underestimated. However this is misleading, because these two relations describe *how* Es are distributed on the FP and so, even if characterized by a larger scatter than the edge-on view of the FP, they contain important information on the galactic properties. The proposed original form of the FJ relation was $L_B \propto \sigma_0^n$, with $n \approx 4$, while Davies et al. (1983) found that the double-slope fit

$$\frac{L_B}{10^{11} L_{B\odot}} \simeq 0.23 \left(\frac{\sigma_0}{300 \text{ km s}^{-1}} \right)^{2.4} + 0.62 \left(\frac{\sigma_0}{300 \text{ km s}^{-1}} \right)^{4.2} \quad (5)$$

provides a better description of the data. Note that for small galaxies and bulges ($\sigma_0 \lesssim 170 \text{ km s}^{-1}$) the exponent is ~ 2.4 ,

* As it is well known, the FP tilt depends on the adopted photometric band. Curiously, when using the k -space, the coefficient in the K-band is only slightly different from 0.15, with a reported value of 0.147 (Pahre, Djorgovski & de Carvalho 1998b).

considerably smaller than 4; this situation is also reflected by the fit of Dressler et al. (1987) to the galaxies of Virgo cluster, $L_B \propto \sigma_0^{3.5}$. Due to indeterminacy of the exact value of n , in the rest of the paper we use 3.5 and 4 as representative values of the FJ exponent.

The total luminosity of spheroidal systems also correlates with their length scale as measured by $\langle R \rangle_e$: in fact, the Kormendy relation can be written in the form

$$\langle R \rangle_e \propto L_B^a, \quad (6)$$

where the exponent a is strongly dependent on the galaxy sample used, and is found in the range $0.88 \lesssim a \lesssim 1.62$ (Ziegler et al. 1999). The latest estimates seem to converge to a value $a \sim 0.7$ or less, as a function of waveband (Bernardi et al. 2003).

In the last years, another important scaling relation has been added to the list, the so-called $M_{\text{BH}}-\sigma_0$ relation (see, e.g., Gebhardt et al. 2000; Ferrarese & Merritt 2000, Merritt & Ferrarese 2001, Tremaine et al. 2002):

$$M_{\text{BH}} \propto \sigma_0^\alpha, \quad (7)$$

where σ_0 is the projected central velocity dispersion of the parent galaxies (or within $\langle R \rangle_e$), and the exact value of α is still matter of debate, ranging between 4 and 5. An important characteristic of this relation is its extremely small scatter, consistent with measurements errors only, so that equation (7) can be considered a “perfect” relation.

In the context of galaxy formation studies, a natural question to ask is how well *dissipationless* merging is able to produce and maintain these relations. We focus on dissipationless merging since it is simpler to be modeled with respect to gas rich merging, and because in this way we can check whether the contribution of gas dissipation is required in the merging scenario of Es formation. In addition, the analysis of dissipationless merging should indicate whether the merging between gas poor systems observed at $z < 1$ (van Dokkum et al. 1999) is a common phenomenon in Es lifetime, or a rare event. Among others, existence of serious problems encountered by the picture of Es formation mainly driven by dissipationless merging to reproduce their scaling relations was pointed out by Ciotti & van Albada (2001; hereafter CvA). In their *phenomenological approach*, just by combining the observed (edge-on) FP and the $M_{\text{BH}}-\sigma_0$ relations, they demonstrated that in a dissipationless merging scenario, and under reasonable assumptions for the addition of BH masses during the merging, *elliptical galaxies forced to lie on the FP and to satisfy the $M_{\text{BH}}-\sigma_0$ relation* would have effective radii exceedingly larger than those observed in real Es.

Here we follow a complementary approach, and the main goal is verifying, by using high resolution N-body numerical simulations of one and two-component galaxy models, whether the end-products of merging of galaxies, initially lying on the FP, lie on the FP (as well as on the other scaling relations) or they fail in some other respect (see also Pentericci, Ciotti & Renzini 1995; Capelato, de Carvalho & Carlberg 1995; Bekki 1998; Evstigneeva, Reshetnikov & Sotnikova 2002; Nipoti, Londrillo & Ciotti 2003a).

Numerical simulations are needed since, owing to possible structural and/or dynamical non-homology and to projection effects, one cannot predict with simple theoretical arguments how σ_0 and $\langle R \rangle_e$ evolve as consequence of merg-

ing: however, rough indications on their behavior can be derived from the study of the evolution of the *virial velocity dispersion* σ_V and the *virial radius* r_V^\dagger . In fact, as a consequence of the virial theorem and the conservation of the total energy, in the merging of two galaxies with masses M_1 and M_2 and virial velocity dispersions $\sigma_{V,1}$ and $\sigma_{V,2}$, the virial velocity dispersion of the resulting galaxy (in case of no mass loss and negligible kinetic and interaction energies of the galaxy pair when compared to their internal energies) is given by

$$\sigma_{V,1+2}^2 = \frac{M_1\sigma_{V,1}^2 + M_2\sigma_{V,2}^2}{M_1 + M_2}. \quad (8)$$

It follows that $\sigma_{V,1+2} \leq \max(\sigma_{V,1}, \sigma_{V,2})$, i.e., *the virial velocity dispersion cannot increase in a merging process of the kind described above*. Under the same hypotheses, the virial radius $r_{V,1+2}$ of the resulting galaxy is given by

$$\frac{(M_1 + M_2)^2}{r_{V,1+2}} = \frac{M_1^2}{r_{V,1}} + \frac{M_2^2}{r_{V,2}}, \quad (9)$$

where $r_{V,1}$ and $r_{V,2}$ are the virial radii of the progenitors. Identity (9) implies that

$r_{V,1+2} \geq \min(r_{V,1}, r_{V,2})$, i.e., *the virial radius cannot decrease in a merging process of the kind described above*.

From equations (8) and (9) it follows that, in the highly idealized scenario of a merging hierarchy based on identical, one-component seed galaxies characterized by $\sigma_{V,0}$, $r_{V,0}$ and M_0 , we expect $\sigma_V = \sigma_{V,0}$ and $r_V = (M/M_0)r_{V,0}$, independently of the merging sequence. Thus, by qualitatively assuming that $\sigma_0 \sim \sigma_V$ and $\langle R \rangle_e \sim r_V$, one should conclude that the FJ and Kormendy relations are not consistent with the scenario depicted above. Now, it is well known that for a large variety of mass models there is a good correlation between r_M (the half-mass radius of the galaxy, strictly related to $\langle R \rangle_e$) and r_V , with the proportionality constant showing little dependence on the particular density profile[†] (see, e.g., Spitzer 1969, Ciotti 1991), and so, even in presence of structural non-homology in the merging end-products, the “prediction” of a linear growth of $\langle R \rangle_e$ with M should be quite robust. A more problematic situation (that can be properly addressed only with numerical simulations) arises when considering the relation between σ_V and σ_0 : at variance with r_M/r_V , structural non-homology can *strongly* affect the ratio σ_0/σ_V (see, e.g., Ciotti, Lanzoni & Renzini 1996; Bertin, Ciotti & Del Principe 2002). In addition, a systematic variation of orbital anisotropy with mass (the so-called dynamical non-homology) can produce an increasing σ_0 even at constant σ_V (although Nipoti, Londrillo & Ciotti 2002, hereafter NLC02, showed that the whole tilt of the FP cannot be ascribed to orbital anisotropy effects only).

Here, with the aid of high-resolution N-body simulations of one and two-component galaxy models, we investigate the effect of subsequent generations of merging on the galaxy scaling relations. Our study explore two extreme situations, namely the case of *major merging*, in which equal

[†] By definition in a one-component galaxy $\sigma_V^2 \equiv 2T/M$ and $r_V \equiv -GM^2/U$, where T and U are the total kinetic and the gravitational energy of the galaxy, respectively.

[‡] For example in truncated power-law spherical models $r_V/r_M = \frac{1}{2^{3-\gamma}}(5-2\gamma)/(3-\gamma)$ and so $2 \leq r_V/r_M \lesssim 2.1$ for $0 \leq \gamma \leq 2$.

mass galaxies are involved at each step of the hierarchy, and the case of *accretion*, in which a massive galaxy increases its mass by incorporating smaller galaxies: the evolution of more realistic, “mixed” merging histories should be bracketed by our simulations. This paper is organized as follows. In Section 2 we describe the properties of the galaxy models and the adopted numerical methods. In Section 3 we present the results, while in Section 4 we specifically discuss the consequences of the findings on the implications for the $M_{\text{BH}}-\sigma_0$ relation. Finally, in Section 5 the main conclusions are summarized.

2 NUMERICAL METHODS

2.1 Galaxy models

As initial conditions for the first generation of merging we use spherically symmetric one and two-component Hernquist density distributions (Hernquist 1990; Ciotti 1996, 1999). This choice is motivated by the fact that the Hernquist model is both a reasonable approximation (when projected) of the $R^{1/4}$ law (de Vaucouleurs 1948), and it is also similar to the Navarro, Frenk & White (1996) profile, thus providing a sufficiently realistic description of the galaxy stellar and dark matter (DM) density distributions. The density, mass, and (relative) potential profiles of the stellar component of the Hernquist model are given by

$$\rho_*(r) = \frac{1}{2\pi} \frac{M_* r_c}{r(r_c + r)^3}, \quad (10)$$

$$\frac{M_*(r)}{M_*} = \left(\frac{r}{r_c + r} \right)^2, \quad (11)$$

$$\Psi_*(r) = \frac{GM_*}{r_c + r}, \quad (12)$$

where M_* is the total stellar mass. In the two-component models, the DM halo is described by ρ_h , M_h and Ψ_h profiles of the same family of equations (10)-(12), where now $r_h \equiv \beta r_c$ and $M_h \equiv \mu M_*$. At variance with the models used in NLC02, here we restrict to globally isotropic models: the distribution function (DF) of the stellar component is then given by

$$f_*(\mathcal{E}) = \frac{1}{\sqrt{8\pi^2}} \frac{d}{d\mathcal{E}} \int_0^\mathcal{E} \frac{d\rho_*}{d\Psi_T} \frac{d\Psi_T}{\sqrt{\mathcal{E} - \Psi_T}}, \quad (13)$$

where $\mathcal{E} = \Psi_T - v^2/2$ is the relative (positive) energy, v is the modulus of the velocity vector, and $\Psi_T = \Psi_* + \Psi_h$ is the relative total potential; an analogous identity holds for the DM halo, where ρ_h substitutes ρ_* .

According to the given definitions, the one-component models are completely determined by the two physical scales M_* and r_c , and in the numerical simulations M_* , r_c and T_{dyn} are adopted as mass, length and time scales. In particular T_{dyn} is the half-mass dynamical time, defined as

$$T_{\text{dyn}} \equiv \sqrt{\frac{3\pi}{16G\rho_M}} \simeq 8.33 \sqrt{\frac{r_c^3}{GM_*}}, \quad (14)$$

where $\rho_M = 3M_*/8\pi r_M^3$ is the mean density inside the half-mass radius r_M . Finally, the velocity scale is given by

$$v_c \equiv \frac{r_c}{T_{\text{dyn}}} \simeq 0.12 \sqrt{\frac{GM_*}{r_c}}. \quad (15)$$

The two–component Hernquist models are characterized by four quantities, the two physical scales M_* and r_c , and the two dimensionless parameters μ and β . In order to transform the results of the numerical simulations in physical units we express M_* in $10^{10}M_\odot$, r_c in kpc, L_B in $10^{10}L_{B\odot}$, and the constant *stellar mass–to–light ratio* $\Upsilon_* \equiv M_*/L_B$ in solar units. For a detailed description of the numerical realization of the initial conditions, see Section 2.1.3 of NLC02.

2.2 Initial conditions

2.2.1 Equal mass merging

The first generation of the *equal mass merging* hierarchy is obtained by merging a pair of identical, spherically symmetric and isotropic Hernquist models (the “zeroth order” seed galaxies), while the successive generations are obtained by merging pairs of identical systems obtained by duplicating the end–product of the previous step. We followed the evolution of the hierarchy of 5 steps of *head–on* mergers (that would correspond, in absence of mass escape, to a mass increase of a factor 32); we also explored 3 steps of the *head–on* merging hierarchy whose seed galaxies are two–component Hernquist models (in which we assume a DM halo more massive, $\mu = 3$, and less concentrated, $\beta = 2$, than the stellar component), and, finally, 3 steps of the hierarchy of encounters of one–component models with *non zero (orbital angular momentum)*.

In the assignment of the initial conditions for the head–on encounters the two galaxies are initially placed on an orbit characterized by vanishing relative energy and angular momentum, i.e., they would have a null relative velocity while at infinite relative distance. In practice, at the time $t = 0$, we place the two galaxies at a distance $d_{\text{rel}} \simeq 3\langle r \rangle_{90}$ (where $\langle r \rangle_{90}$ is the angle–averaged radius enclosing the 90% of the total mass M of each galaxy), and, neglecting the effects due to tidal forces, we assign to their centers of mass a relative velocity with modulus $v_{\text{rel}} = 2\sqrt{GM/d_{\text{rel}}}$. The end–products of each merging are non–spherical, and so, when exploring a successive merging, their mutual orientation at the beginning of the new simulation is randomly assigned. In the simulations with orbital angular momentum, we still consider vanishing relative energy and d_{rel} defined as above, and we assume as impact parameter the sum of the angle–averaged half–mass radii of the merging galaxies.

2.2.2 Accretion

In the case of the merging hierarchy in which the test galaxy grows by accretion of smaller systems (*accretion*), the seed galaxy is a one–component Hernquist model, and the first merging event is identical to that in the equal mass merging case. In the second step, however, the first end–product (of mass $\sim 2M_*$) merges again with a seed galaxy, and so on. As a consequence, the mass ratio between the infalling stellar system and the test galaxy decreases approximately as $1/n$, where n is the step in the accretion hierarchy. Due to the higher computational cost required by accretion simulations with respect to equal mass merging in order to reach the same mass increase, in the former case we limit to 15 steps (of head–on merging) and to 9 steps (of merging with angular momentum), for a putative mass increase of a factor 16

and 10, respectively. As in the case of equal mass merging simulations, the relative initial positions and velocities of the infalling satellite and of the test galaxy are chosen so that at $t = 0$ they are on parabolic orbit, and the mutual orientation of the two galaxies is assigned randomly. In practice, as initial relative distance we adopt $d_{\text{rel}} \simeq \langle r \rangle_{90,1} + 2\langle r \rangle_{90,2}$, where the subscript 2 refers to the smaller galaxy. Again, in case of non zero angular momentum, the impact parameter is given by the sum of the angle–averaged half–mass radii.

2.3 The numerical code

For the simulations we used a new, fast and accurate, parallel N–body code. Recently, a numerical scheme has been introduced to simulate collisionless N–body systems by Dehnen (2000, 2002), with a substantial improvement in force computation over standard tree–based codes. By combining in an original way the Fast Multipole Algorithm (see, e.g., Greengard & Rokhlin 1987, 1997) with the Barnes & Hut (1986) tree data structure, Dehnen scheme achieves exact momentum conservation with an effective $O(N)$ operational complexity (for particle numbers $N \gtrsim 10^5$).

By taking advantage of these improvements, we have implemented the Dehnen fast force solver (FalcON) in a parallel Fortran–90 N–body code named FVFPS (Fortran Version of a Fast Poisson Solver; Londrillo, Nipoti & Ciotti 2003). The FVFPS code is based on domain decomposition, and uses the MPI routines for data communication. A mass dependent opening parameter $\theta = \theta(M)$, that assures faster performances and a more uniform error distribution, is also employed (Dehnen 2002). Time integration is performed by a standard leap–frog algorithm, with (uniform) time step Δt determined adaptively. Thanks to effective $O(N)$ scaling of the force computations, the FVFPS code assures a speed–up of a factor ~ 10 over existing codes, in particular over the Springel, Yoshida & White (2001) GADGET code. In the present version, the FVFPS code is characterized by three preassigned parameters:

(i) The minimum value of the opening parameter θ_{min} , associated with the total mass. We adopt $\theta_{\text{min}} = 0.5$, resulting in mean relative force errors of $\sim 0.3\%$, and 99 percentile errors of $\sim 3\%$.

(ii) The softening parameter ε (i.e., the softening length expressed in units of r_c), dependent, according to literature indications (e.g., Merritt 1996, Athanassoula et al. 2000, Dehnen 2001), on N and on the specific density distribution profile.

(iii) For the initial time step we assume $\Delta t \sim T_{\text{dyn}}/100$. The time step is allowed to vary adaptively as a function of the maximum particle density, but is kept the same for all the particles.

For the stellar distribution of the seed galaxies we use as a rule $N_* = 16378$ particles for each galaxy, and in the two–component cases the DM distribution is made of $N_{\text{DM}} = 49152$ particles: with this choice, halo and stellar particles have the same mass. As a consequence of the merging hierarchy, the number of particles in the simulations increases with the galaxy mass: in the final merging of (one and two–component) equal mass systems and of the accretion scenario, the total number of particles involved is of the order of 5.2×10^5 and 2.6×10^5 , respectively.

We followed the dynamical evolution of each merging

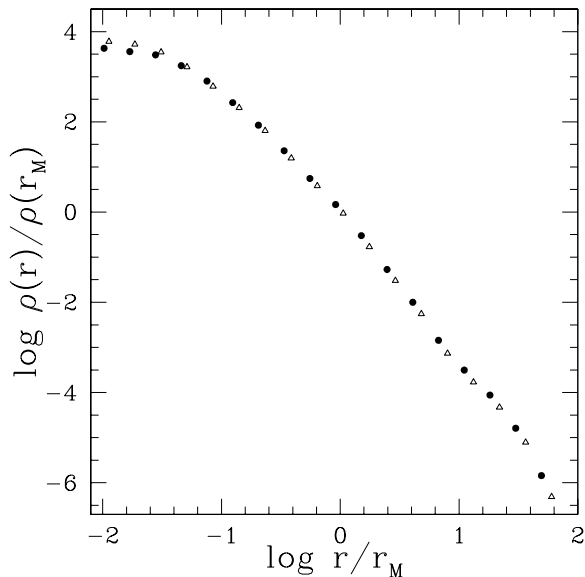


Figure 1. Angle-averaged density as a function of radius (normalized to the half-mass radius r_M) of the end-product of the head-on merging of two one-component Hernquist models, obtained with GADGET (empty triangles) and with the FVFPS code (solid circles).

event up to the virialization of the resulting system, which is usually reached on a time scale shorter than $50T_{\text{dyn}}$ after the first encounter between the two galaxies: for example the virialization time for the first step in the one-component (head-on) equal mass merging hierarchy is of the order of 2 Gyr having assumed $M_* = 10^{10} M_\odot$ and $r_c = 1$ kpc. In the following we call “end-product” of a simulation the system made of bound particles after the virialization. For the determination of the intrinsic and “observational” properties of the end-products, we followed the same procedure described in NLC02. In particular we measured the end-product intrinsic axis ratios c/a and b/a (where a , b and c are the major, intermediate and minor axis of the associated inertia ellipsoid), their virial velocity dispersion σ_V and angle-averaged half-mass radius r_M , and, for several projection angles, the end-product circularized effective radius $\langle R \rangle_e$, the central velocity dispersion σ_0 , and the mean effective surface brightness $\langle I \rangle_e$ (obtained from the stellar mass profile by assuming a constant stellar mass-to-light ratio Υ_*). In particular, the central velocity dispersion σ_0 is obtained by averaging the projected velocity dispersion over the circularized surface brightness profile within a radius of $\langle R \rangle_e/8$. As a general rule we find that discreteness effects on the derived values of $\langle R \rangle_e$ and σ_0 do not exceed $1 \div 2\%$ at each projection angle.

We checked the reliability of the numerical simulations by running a few merging events both with the parallel version of GADGET (with $\alpha = 0.02$, $\Delta t_{\text{min}} = 0$, $\Delta t_{\text{max}} = T_{\text{dyn}}/100$, $\alpha_{\text{tol}} = 0.05$, and $\varepsilon = 0.05$; see Springel et al. 2001 for details) and with our FVFPS code (with $\theta_{\text{min}} = 0.5$, $\varepsilon = 0.05$ and $\Delta t = T_{\text{dyn}}/100$). The results are in remarkable agreement: the end-products in three-dimensional shape, angle-averaged half-mass radius, density and velocity dispersion profiles are practically indistin-

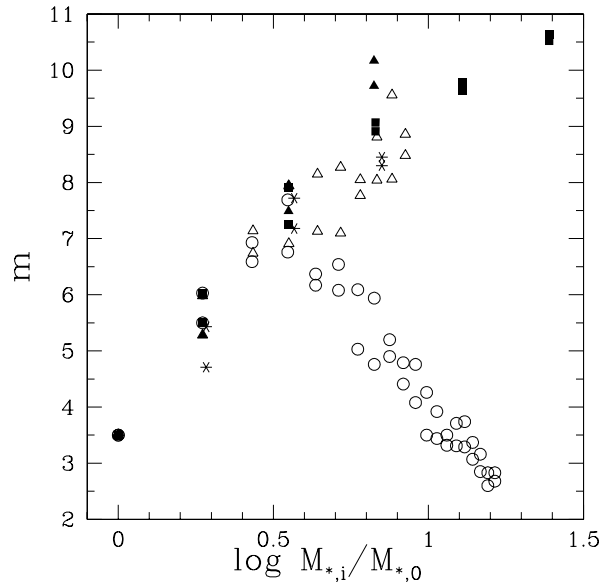


Figure 2. Sersic best fit parameter m vs. total stellar mass of the end-products at stage i of the merging hierarchy. Equal mass mergers are shown as solid triangles and squares (one-component galaxies), and stars (two-component galaxies); empty triangles and circles represent the accretion hierarchies. Triangles correspond to simulations with non zero orbital angular momentum.

guishable. With both codes the total energy is conserved within 1% over 100 dynamical times. As an illustrative example, in Fig. 1 we show the density profiles of the end-products of the head-on merging of two Hernquist models (GADGET, empty triangles; FVFPS, solid circles); note how “minor” details, as the slope change in the density profile at $r \sim 10r_M$, are nicely reproduced. All the simulations were run on a Cray T3E, and on a IBM Linux Cluster (with a number of processors from 4 up to 32, depending on the number of particles of the simulation).

3 THE RESULTS

3.1 Equal mass merging

Before presenting the effects of equal mass merging on the FP and on the other scaling relations, we briefly describe the induced modifications of the internal structure and dynamics of one and two-component galaxy models. In general, the end-products are triaxial systems with axis ratios in the range $0.5 \lesssim c/a \lesssim 0.7$ and $0.7 \lesssim b/a \lesssim 0.8$ (where a , b and c are the major, intermediate and minor axis, respectively), in accordance with observed ellipticities of Es. For comparison with real galaxies, we also fitted (over the radial range $0.1 \lesssim R/\langle R \rangle_e \lesssim 10$) the projected stellar mass density profile of the end-products with the Sersic (1968) $R^{1/m}$ law:

$$I(R) = I_0 \exp \left[-b(m) \left(\frac{R}{R_e} \right)^{1/m} \right], \quad (16)$$

where $b(m) \simeq 2m - 1/3 + 4/405m$ (Ciotti & Bertin 1999), and in Fig. 2 we plot the best fit parameter m as a function of the total mass of the systems, for one-component (solid squares and triangles) and two-component (stars) models. Clearly,

the fitted quantities m and $\langle R \rangle_e$ depend on the relative orientation of the line-of-sight and of the end-products of the simulations: the two points for each value of the mass in Fig. 2 show the range of values spanned by m when projecting the final states along the shortest and longest axis of their inertia ellipsoids. We note that higher values of the best fit parameter m correspond to more massive systems, a trend similar to that observed in Es[§] (see, e.g., Caon, Capaccioli & D’Onofrio 1993, Prugniel & Simien 1997, Bertin et al. 2002). Note also that the values of m are in the same range obtained from observations, in fact we found $2 \lesssim m \lesssim 11$. (However, as pointed out to us by the Referee, from Fig. 2 one could argue that $m \approx 4$ galaxies should have experienced at most one major merger event in their life.)

Following the discussion in the Introduction, in Fig. 3 (top panel) we show the relation between the virial velocity dispersion and the total stellar mass of the mergers at each step of the merging hierarchy. In one-component models (solid squares and triangles) a modest increase of σ_V with M_* is apparent: for the last model in the hierarchy the mass is increased by a factor ~ 24.5 (instead of the maximum possible value of 32), while the σ_V is increased by a factor ~ 1.16 only. This small increase of σ_V with respect to the expectation of equation (8) (i.e., $\sigma_V = \text{const}$) can be explained with a simple generalization of the highly idealized situation formalized there. In fact, if during a merging between two galaxies with mass M_1 , M_2 and virial velocity dispersion $\sigma_{V,1}$, $\sigma_{V,2}$ a mass ΔM is lost with mean velocity v_{ej} , then the virial velocity dispersion of the end-product $\sigma_{V,1+2}$ is expected to be

$$\sigma_{V,1+2}^2 = \frac{M_1 \sigma_{V,1}^2 + M_2 \sigma_{V,2}^2 + \Delta M v_{ej}^2}{M_1 + M_2 - \Delta M} \quad (17)$$

in particular σ_V increases as a consequence of the mass (and associated kinetic energy) loss. We found that in the simulations the mass lost during each merging never exceeds $\Delta M / (M_1 + M_2) \simeq 0.06$ and, consistently, the corresponding increase of σ_V is $2 \div 5\%$ (Fig. 3, top panel).

In Fig. 3 (bottom panel) we plot the half-mass radius as a function of the stellar mass of the mergers. As for σ_V , also for this quantity the simple virial expectation of a linear growth of r_V (and of r_M) with M (dotted line) is apparent. The “jump” from the initial condition position to the first merger is due to the significant change in the galaxy density structure (as revealed by the change of values of m in Fig. 2); the successive generations of merging are characterized by more similar density profiles, and, correspondingly, the points in Fig. 3 move parallel to the dotted line.

How does the presence of massive DM halos affect these results? As anticipated, in this case we investigated 3 steps of the (head-on) equal mass merging hierarchy by using two-component galaxy models. Due to its observational relevance, we focus here on the description of the properties of the stellar component only. As in the one-component case, the end-products are triaxial, and with the axis ratios in the same range. The best fit Sersic parameter m still in-

creases with mass (stars in Fig. 2). In the two-component simulations, owing to the presence of the DM halo, there are not arguments as simple as those used in equations (8), (9) and (17) in order to predict the effects of merging on σ_V (defined as $2T_*/M_*$) and r_M of the *stellar* component. However, it is apparent from Figs. 2 and 3 that the presence of a DM halo or angular momentum in the initial conditions does not modify the general trend of m , σ_V and r_M at increasing mass.

3.1.1 Fundamental Plane

In Fig. 4 we plot the results of equal mass merging simulations in the principal planes (k_1, k_3) and (k_1, k_2) , where one-component galaxy models resulting from head-on mergers and from merging with angular momentum are identified by solid squares and triangles, respectively; two-component models are represented by stars. The progenitor of the merging hierarchy (the point without bar) is placed on the edge-on FP by choosing its luminosity $L_B = 3 \times 10^9 L_{B\odot}$ and stellar mass-to-light ratio $\Upsilon_* = 5$, so that equation (4), represented by the solid line, is satisfied. Consistently with the adopted dissipationless scenario, the value of Υ_* is kept constant during the whole merging hierarchy. Due to the loss of spherical symmetry of the end-products of the merging simulations, their coordinates depend on the line-of-sight direction; however, being the luminosity (mass) of each end-product fixed, variations of k_1 , k_2 , k_3 due to projection effects are not independent. In fact, the k_1 and k_3 coordinate of a galaxy of given luminosity are linearly dependent as

$$k_3 = \sqrt{\frac{2}{3}} k_1 + \sqrt{\frac{1}{3}} \log \frac{2\pi}{L_B} \quad (18)$$

this dependence is reflected by the straight lines in Fig. 4 (top panel), each of them representing the range spanned in the (k_1, k_3) space by a given end-product when observed over the solid angle. As in NLC02, in order to quantify the deviation of a model from the FP, we use the vertical distance $\delta k_3 \equiv |k_3 - 0.15k_1 - 0.36|$ from the point to the FP itself. It is interesting to note that for all the end-products the projection effects translate into a δk_3 of the same order of magnitude of the observed FP dispersion. In addition it is also apparent from Fig. 4 how k_3 and k_1 increase with the galaxy mass consistently with the observed FP tilt and thickness. Being Υ_* fixed in our simulations, from Fig. 2 we conclude that one-component equal mass dissipationless merging is able to reproduce (basically by structural non-homology) the edge-on FP of elliptical galaxies (see also Capelato et al. 1995).

We also explored the behavior of the models in the (k_1, k_2) plane (Fig. 4, bottom panel), which represents the face-on view of the FP; the region populated by real galaxies in this plane is identified by dashed lines. By fixing the scale length, we place the first progenitor (with $\langle R \rangle_e \simeq 0.7$ kpc) in a zone of the (k_1, k_2) plane populated by low-luminosity ellipticals ($k_1 \simeq 3$, $k_2 \simeq 4.5$), and for each end-product we plot the (k_1, k_3) positions for a few random projection angles. Note that, at variance with the coordinates (k_1, k_3) , k_1 and k_2 are related (for a given end-product) by an expression containing $\langle R \rangle_e$ besides L_B , and for this reason in the (k_1, k_2) plane the effect of projection is to distribute the

[§] Curiously, NLC02 found that in the case of end-products of unstable galaxy models m decreases for increasing radial orbital anisotropy in the initial conditions. Note also that in NLC02 and Londrillo et al. 2003 we used a radial range $0.1 \lesssim R / \langle R \rangle_e \lesssim 4$.

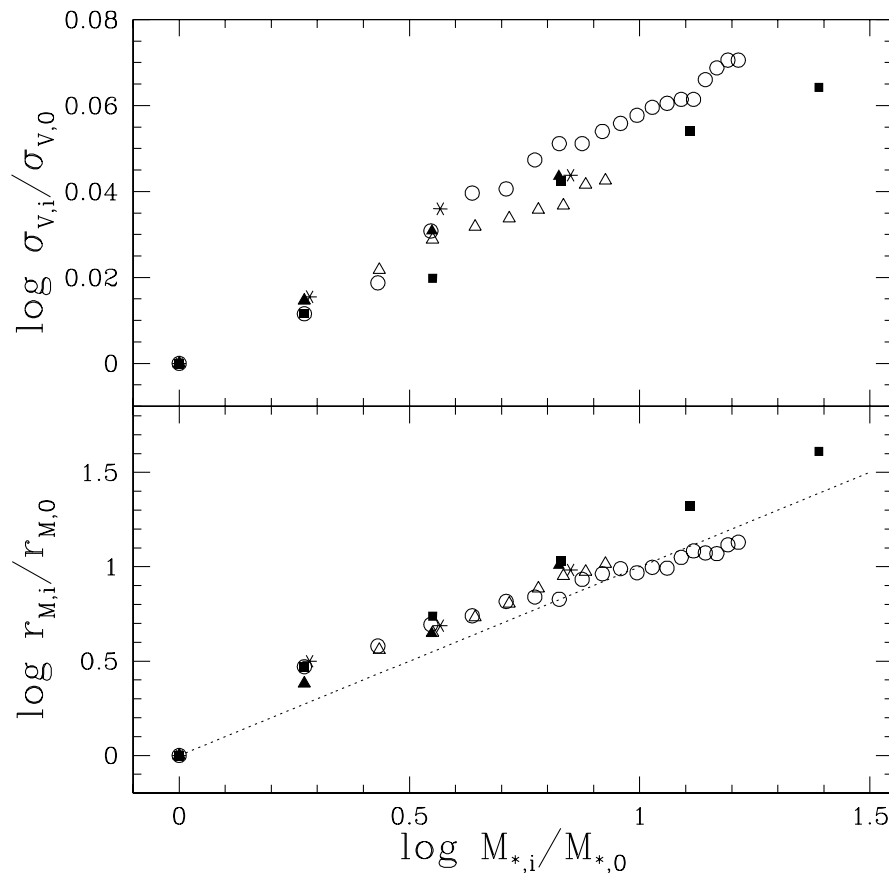


Figure 3. *Top panel:* virial velocity dispersion of the stellar component at stage i of the merging hierarchy vs. the total stellar mass of the merger. *Bottom panel:* angle-averaged half-mass radius r_{M} vs. total stellar mass. Symbols are the same as in Fig. 2. The dotted line indicates the relation $r_{\text{M}} \propto M$; $M_{*,0}$, $r_{\text{M},0}$ and $\sigma_{\text{V},0}$ are the stellar mass, the virial velocity dispersion and the half-mass radius of the seed galaxy. In the two-component cases, σ_{V} and r_{M} refer to the stellar component only. Note the different range spanned in the ordinate axes in the two panels.

end-products on two-dimensional regions. One-component equal mass mergers (solid squares and triangles) are moved by merging towards the bottom right of the (k_1, k_2) plane, roughly parallel to the line defining the *zone of avoidance*, in accordance with the prediction of BBF. The produced displacements are very large: it is remarkable that the end-products of the last step of the hierarchy are found in a position only marginally consistent with the populated region in the (k_1, k_2) space. It is also interesting to note that the presence of substantial angular momentum in the initial conditions does not change significantly the properties of equal mass mergers, both in the (k_1, k_3) and in the (k_1, k_2) plane.

The results of equal mass merging of two-component galaxies are represented in Fig. 4 with stars. Due to the presence of DM, in order to place the first progenitor ($L_{\text{B}} = 3 \times 10^9 L_{\text{B}\odot}$) on the FP, we assumed a stellar mass-to-light ratio $\Upsilon_* = 2.3$. It is apparent that both in the (k_1, k_3) and (k_1, k_2) planes, the behavior of two-component models does not significantly differ from the corresponding one-component models. In other words, *dissipationless, equal mass merging of one and two-component models seems to be consistent with the existence of the FP of Es.*

3.1.2 Faber–Jackson and Kormendy relations

As we have shown in the Section above, dissipationless merging of one and two-component galaxy models is surprisingly consistent with the existence of the FP, especially considering its small thickness when seen edge-on. However, Es do follow additional scaling relations as the FJ and Kormendy relations, and so here we compare the results of our simulations with these scaling laws.

The solid line in the upper panel of Fig. 5 represents the FJ relation in the form $L_{\text{B}} \propto \sigma_0^4$ together with its scatter ($\delta \log \sigma_0 \simeq 0.1$, Davies et al. 1983, dashed lines); the dotted line represents the steeper fit ($L_{\text{B}} \propto \sigma_0^{3.5}$) derived by Dressler et al. (1987). The end-products of (head-on) equal mass merging of one-component galaxies (solid squares) have a σ_0 lower than that predicted by the FJ relation for the given mass increase, and the discrepancy is stronger in case of merging with angular momentum (solid triangles). It is interesting to compare this plot with the upper panel of Fig. 3: it is then clear how the failure of FJ can be directly traced to the constancy of σ_{V} and to the significant dynamical homology of the mergers. This latter point again suggest that *structural non-homology*, more than dynamical non-homology is at the origin of the FP in the explored merging

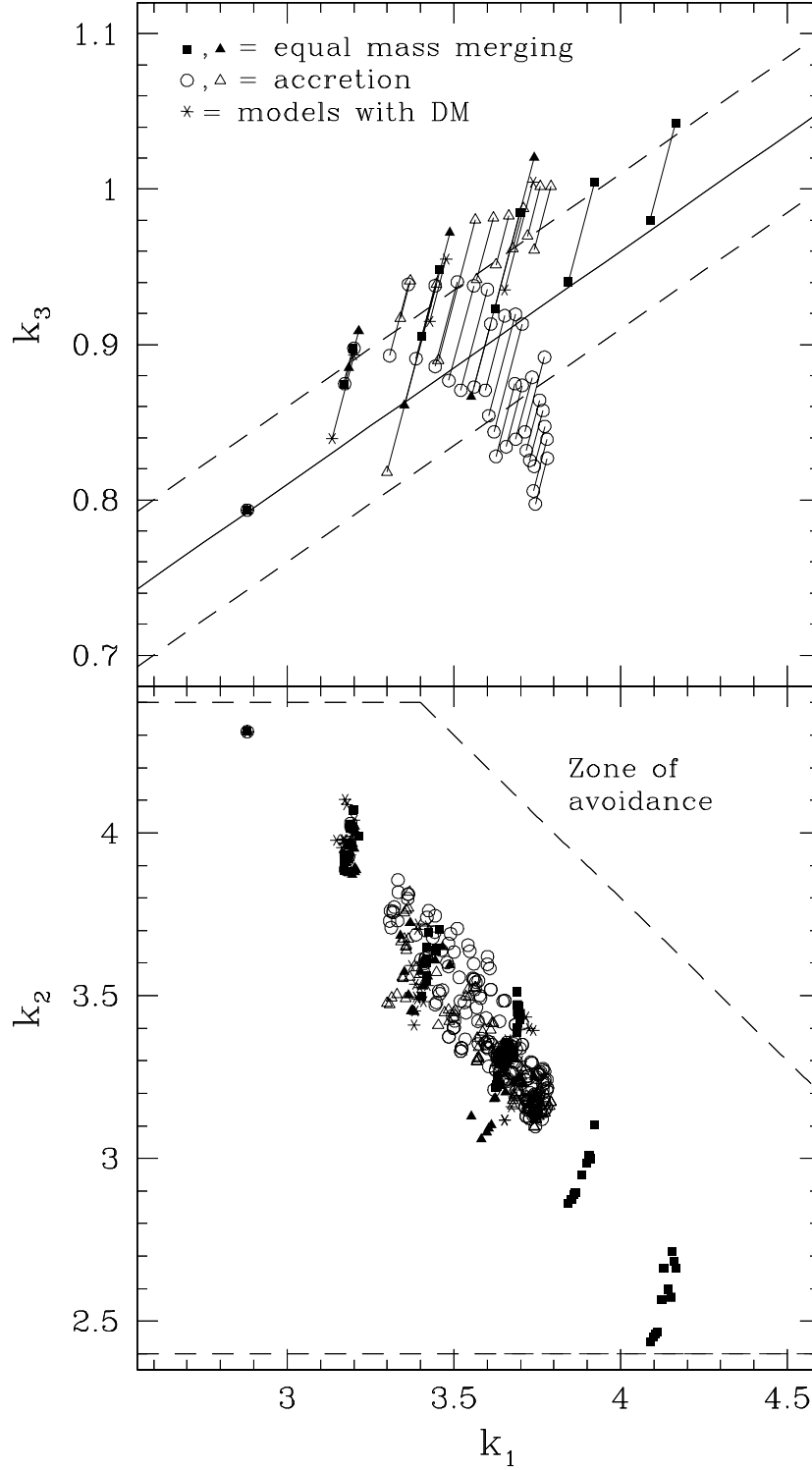


Figure 4. *Top panel:* the merging end-products in the (k_1, k_3) plane, where the solid line represents the FP relation as given by equation (4) with its observed $1\text{-}\sigma$ dispersion (dashed lines). Bars show the amount of projection effects. *Bottom panel:* the merging end-products in the (k_1, k_2) plane, where the dashed lines define the region populated by real galaxies as given by BBF. Each model is represented by a set of points corresponding to several random projections. Symbols are the same as in Fig. 2.

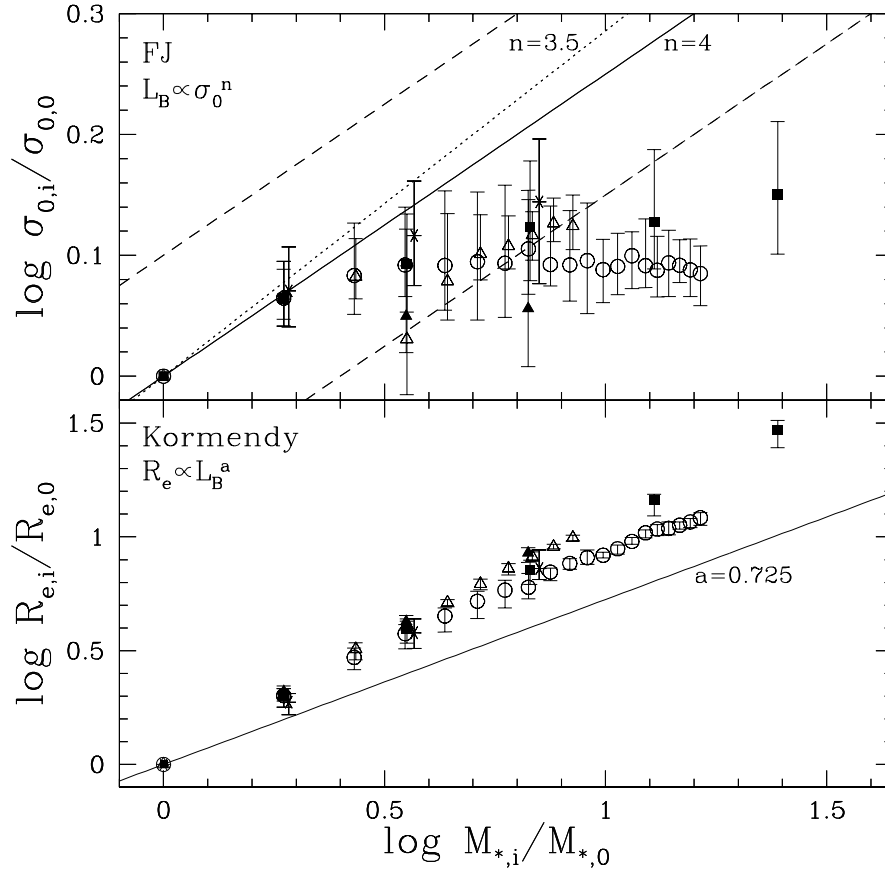


Figure 5. *Top panel:* stellar central velocity dispersion (normalized to that of the first progenitor) vs. total stellar mass. Points correspond to angle-averaged values, bars indicate the range spanned by projection effects. The solid and the two dashed lines represent the Faber-Jackson relation $L_{\text{B}} \propto \sigma_0^4$ and its scatter, while the dotted line represents $L_{\text{B}} \propto \sigma_0^{3.5}$. *Bottom panel:* stellar effective radius (normalized to that of the first progenitor) vs. total stellar mass. Points and bars have the same meaning as in top panel. The solid line represents our “fiducial” Kormendy relation, obtained combining the FP and the FJ with $n = 4$ (see text); symbols are the same as in Fig. 2. Note the different range spanned in the ordinate axes in the two panels.

scenario (see also NLC02). Models with DM (stars in Fig. 5) seem to follow more closely the FJ relation, even though the representative points show the same clear trend as the one-component merging hierarchy: it seems clear to us that additional simulations would bring also two-component models completely outside the FJ relation.

Considering now the agreement with the FP on one side, and the failure at reproducing the FJ relation on the other side, we would expect that also the Kormendy relation is not reproduced by the equal mass merging hierarchy. In fact, if we assume that the Es obey to the FJ relation, $L_{\text{B}} \propto \sigma^n$, then from equation (4) we obtain a fiducial Kormendy relation $\langle R \rangle_{\text{e}} \propto L_{\text{B}}^{1.225-2/n}$. For example, with $n = 4$ (for which the exponent is remarkably near to that reported by Bernardi et al. 2003) the effective radius of the end-product of the last equal mass merger is a factor ~ 3 larger than that predicted by the “Kormendy” relation. In other words, the results of our simulations are characterized by too large effective radii (see Fig. 5, bottom panel). Thus, in the explored equal mass merging hierarchies both σ_0 and $\langle R \rangle_{\text{e}}$ deviate systematically from the values expected from FJ and Kormendy relations. Yet, their deviations from the two scal-

ing laws curiously compensate reproducing the edge-on FP; this shows clearly that the FJ and Kormendy relations are not simple projections of the FP, which is actually preserved by merging, but, despite their larger scatter, contain additional information on galaxy structure and dynamics.

3.2 Accretion

In Section 3.1 we showed that, in the case of equal mass merging of one and two-component galaxies, the virial expectations were qualitatively followed also by the observational properties $\langle R \rangle_{\text{e}}$ and σ_0 , in addition to σ_{V} and r_{V} . We recall that these expectations are independent of the specific merging history, as far as the zeroth order seed galaxies are identical systems, and so we could consider “accretion” simulations superfluous. However, the amount of escaping particles or the non-homology of the final end-products could depend on the mass ratio of the merging systems, thus resulting in substantial changes in σ_{V} and/or σ_0 . Following this argument we now present the results of accretion simulations, whose technical setting is described in Section 2. From the structural point of view, the end-products of ac-

cretion are less flattened than the corresponding (i.e. with the same mass) equal mass mergers, being, in general, triaxial systems with axis ratios in the range $0.6 \lesssim c/a \lesssim 0.9$, and $0.7 \lesssim b/a \lesssim 0.9$, and becoming more and more spherical with increasing mass as a consequence of the higher number of merging events and the random direction of accretion. The evolution of the surface brightness profile in the accretion hierarchy is shown in Fig. 2, where the best fit Sersic parameter m is represented with empty circles and triangles (for head-on merging and merging with angular momentum, respectively). *A first relevant difference with the equal mass merging results is the decrease of m with mass at mass ratios larger than 4 for the head-on accretions*, and the consequent smaller range of m ($2 \lesssim m \lesssim 8$) spanned by their end-products. Therefore, the explored head-on accretion scenario fails at reproducing the relation between the surface brightness profile shapes and luminosity of real galaxies, which are characterized by m increasing with galaxy luminosity and also spanning a larger range. A different situation is obtained when considering accretion simulations with non negligible orbital angular momentum: the structural properties of the end-products are curiously similar to the equal mass cases.

In the upper panel of Fig. 3 we plot σ_V as a function of mass of also of the head-on accretion end-products (empty circles). We found that the fraction of mass lost in each merging $\Delta M/(M_1 + M_2)$, decreases from ~ 0.06 in the first step to ~ 0.01 in the last one, summing up to a total amount of mass lost over 15 steps of $\sim 18\%$, about the same value found in the corresponding equal mass merging cases. The slightly larger increase of σ_V in the head-on accretion hierarchy with respect to the equal mass merging cases is fully accounted for larger values of v_{ej} , in accordance with the estimate given in equation (17). In the lower panel of Fig. 3 we also show the evolution of r_M in the head-on accretion hierarchy (empty circles). The behavior of this quantity is qualitatively similar to that of equal mass mergers: the slightly flatter slope of the sequence with respect to the simple expectation $r_M \propto M$ is due to the stronger evolution of structural non-homology, as revealed by Fig. 2. On the other hand, the end-products of accretion simulations with angular momentum (empty triangles in Fig. 3) are more similar to equal mass merging case.

3.2.1 Fundamental Plane

The most striking difference of the end-products of head-on accretion simulations (empty circles) with respect to the equal mass merging hierarchy and also to accretion simulations with angular momentum (empty triangles) is apparent in the upper panel of Fig. 4, where the results are plotted in the (k_1, k_3) space. In fact, after few accretions, the end-products are characterized by a k_3 decreasing for increasing k_1 , at variance with the FP slope and the trend shown by the end-products of equal mass mergers. As a consequence, the last explored models (corresponding to an effective mass increase of a factor ~ 12) are found at a distance δk_3 larger than the FP scatter. This result, when interpreted by using the information in Fig. 2, is not surprising. In fact, being the coordinate k_3 a measure of non-homology for galaxies with constant Υ_* (as those explored in this paper), the decrease of the Sersic parameter m at increasing mass (at variance

with real galaxies) reflects directly in the unrealistic trend in the (k_1, k_3) plane. On the contrary, in the face-on (k_1, k_2) plane (Fig. 4, lower panel), the end-products of accretion (both head-on and with angular momentum) evolve along the same direction followed by equal mass mergers, albeit with a smaller excursion in k_1 and k_2 .

3.2.2 Faber–Jackson and Kormendy relations

In Fig. 5 we also plot the results of accretion simulations in the planes representing the FJ and the Kormendy relations. At variance with the case of the edge-on FP, and *independently on the presence of angular momentum*, the behavior of the end-products is considerably similar to that of the equal mass mergers, i.e., both FJ and Kormendy relations are *not* reproduced. The end-products have σ_0 smaller and $\langle R \rangle_e$ larger than the values predicted by the two scaling relations for the given luminosity (mass) increase. However, a closer inspection of Fig. 5 reveals that both σ_0 and $\langle R \rangle_e$ are systematically larger in the case equal mass mergers than in the case of head-on accretion: in other words, the end-products in the latter case deviate *more* from the FJ and *less* from the Kormendy than those in the former. The result relative to the effective radius simply reflects the different evolution of the half-mass radius in the two scenarios (see Fig. 3, lower panel), while the behavior of σ_0 depends both on structural and dynamical non-homology effects: the combined effect of the lower values of σ_0 and the larger values of $\langle R \rangle_e$ is responsible of the decreasing of k_3 with k_1 observed in the analysis of the edge-on FP. In other words, at variance with equal mass mergers and accretions with angular momentum, there is not enough compensation between the trends in σ_0 and $\langle R \rangle_e$ able to reproduce the FP tilt in case of head-on accretions.

4 DISSIPATIONLESS MERGING AND THE $M_{BH}-\sigma_0$ RELATION

On the basis of the results of the previous Section, it is particularly interesting to investigate whether dissipationless merging is able to reproduce the $M_{BH}-\sigma_0$ relation, and we attempt to answer this question by using the simulations presented in Section 3. Here we recall that in our simulations we do not take into account the presence BH in the merging galaxies, yet we argue that we can reach robust conclusions, and this for two reasons. In fact, as well known, at the equilibrium (i.e. after the virialization of the end-product) the presence of the BH has not significant influence on σ_0 . This can easily be seen by considering that the sphere of influence of a BH with mass M_{BH} at the center of a galaxy with central velocity dispersion σ_0 has a fiducial radius $r_{BH} \equiv GM_{BH}/\sigma_0^2$, and combining this equation with equation (7) we obtain

$$r_{BH} \simeq 0.01 \times \left(\frac{\sigma_0}{200 \text{ km s}^{-1}} \right)^{\alpha-2} \text{ kpc}, \quad (19)$$

where we assumed $M_{BH} = 10^8 M_\odot$ when $\sigma_0 = 200 \text{ km s}^{-1}$ (see, e.g., Tremaine et al. 2002). The central velocity dispersion used in the definition of the FP and of the $M_{BH}-\sigma_0$ relations is the luminosity weighted projected velocity dispersion inside the radius $\langle R \rangle_e/8$ which, for ellipticals with $\sigma_0 \simeq 200 \text{ km s}^{-1}$, is in the range $0.2 \lesssim \langle R \rangle_e/8 \lesssim 0.6 \text{ kpc}$,

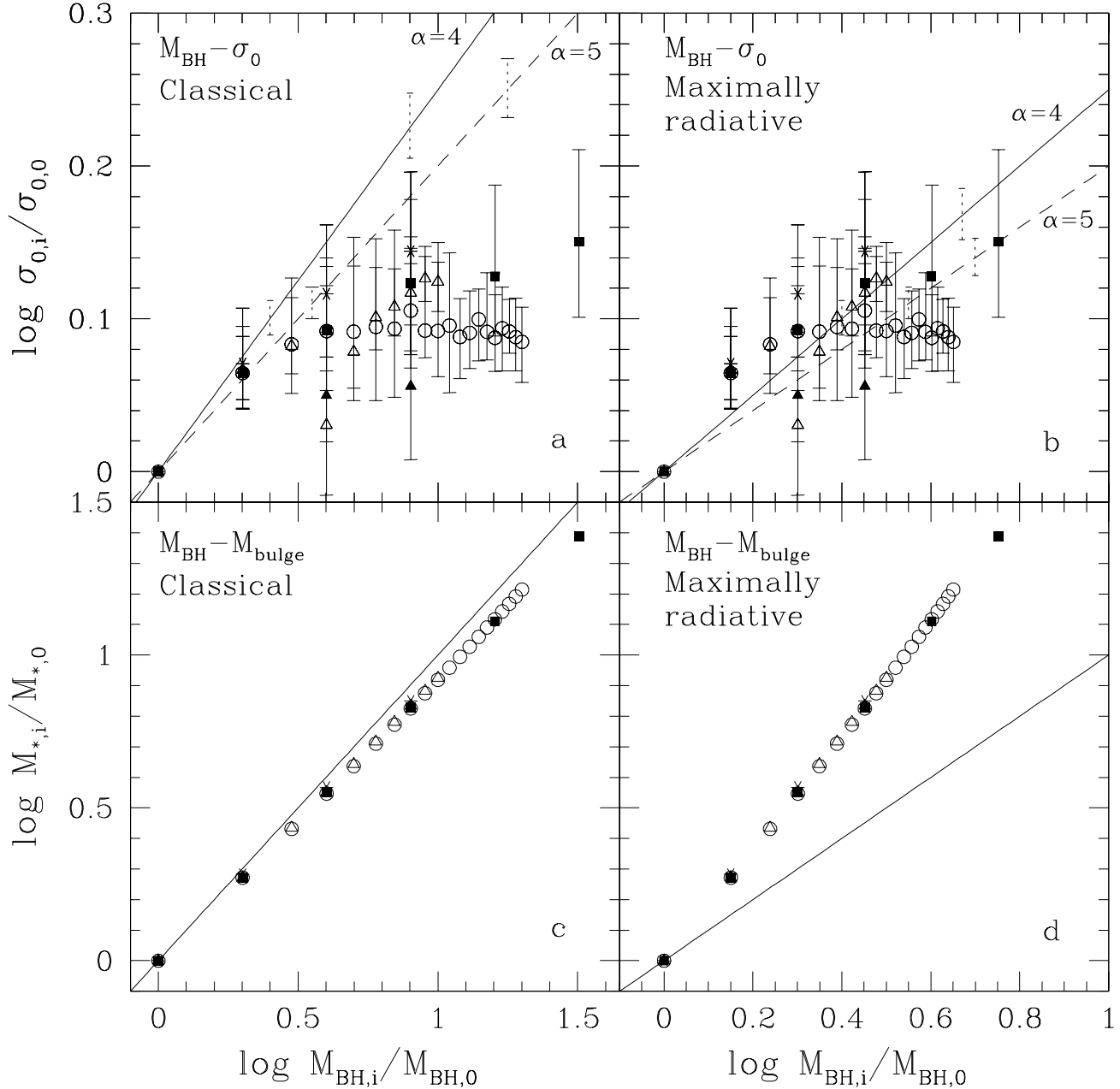


Figure 6. *Panel a:* galactic central velocity dispersion vs. BH mass for classical BH merging; $\sigma_{0,0}$ and $M_{\text{BH},0}$ are the central velocity dispersion and BH mass of the first progenitor, respectively. The points correspond to the mean value over the solid angle, while the bars indicate the range spanned by projection effects. Solid and dashed lines represent the $M_{\text{BH}}-\sigma_0$ relation for $\alpha = 4$ and $\alpha = 5$, respectively, while vertical dotted lines show the observed scatter around these best fits. *Panel b:* same data as in panel a, but for maximally radiative BH merging. *Panel c:* stellar mass vs. BH mass for classical BH merging; $M_{*,0}$ is the stellar mass of the first progenitor and the solid line represents the Magorrian ($M_{\text{BH}} \propto M_{\text{bulge}}$) relation. *Panel d:* same data as panel c, but for maximally radiative BH merging. Symbols are the same as in Fig. 2.

one order of magnitude larger than r_{BH} . Thus, once the numerical end-products reached the equilibrium, their σ_0 is a good estimate of the real quantity even in presence of a BH of realistic mass. The second reason requires a more careful discussion. In fact, during the dynamical evolution of the merging system, a BH binary is formed and, in principle, its evolution could affect the kinematic properties of the end-

product even beyond r_{BH} . However Milosavljevic & Merritt (2001), with the aid of numerical simulations, showed that the formation of a BH binary does not modify significantly the central velocity dispersion measured within the standard aperture $\langle R \rangle_e/8$, although the inner density profile *is* modified (for interesting observational evidences of this case see Lauer et al. 2002). In any case, we remark here that, if any,

the expected effect of binary BHs is to *decrease* the central velocity dispersion, as a consequence of dynamical friction heating against background stars.

On the basis of these considerations we simply assume that each seed galaxy contains a BH of mass $M_{\text{BH},0}$, and that each merging end-product contains a BH obtained by the merging of the BHs of the progenitors (at the end of this Section, however, we will discuss two important problem faced by this last assumption). Unfortunately, BH merging is still a poorly understood physical process, in particular with respect to the amount of emitted gravitational waves (see, e.g., CvA, and references therein), and for this reason we consider two extreme situations: the case of *classical* combination of masses ($M_{\text{BH},1+2} = M_{\text{BH},1} + M_{\text{BH},2}$, with no emission as gravitational waves), and the case of *maximally efficient radiative merging* ($M_{\text{BH},1+2}^2 = M_{\text{BH},1}^2 + M_{\text{BH},2}^2$, corresponding to entropy conservation in a merging of two non rotating BHs). Following this choice, in Fig. 6 we plot the central velocity dispersion of the mergers versus the mass of their central BH in the case of classical (panel a) and maximally radiative (panel b) BH merging. As expected from the similarity between the FJ and the $M_{\text{BH}}-\sigma_0$ relations, in the classical case, both (one-component) equal mass mergers (solid squares and triangles) and accretion mergers (empty circles and triangles) are unable to reproduce the observed relation, even when its slope is assumed as high as 5, with representative points well outside the observed scatter (vertical dotted bars). As it happens for the FJ relation, the situation is somewhat better when considering equal mass mergers of two-component galaxy models: in presence of DM the stellar central velocity dispersion is higher for given BH mass and the end-products are found closer to the observed relation (stars in Fig. 6). Thus, as for the FJ, the reason of the failure of dissipationless merging at reproducing the $M_{\text{BH}}-\sigma_0$ relation is that the end-products are characterized by a too low σ_0 for the given M_{BH} , i.e., M_{BH} is too high for the resulting σ_0 . A promising solution to this problem could be the emission of some fraction of M_{BH} as gravitational waves. In fact, by assuming maximally efficient radiative BH merging, the points are found remarkably closer to the observed relation, even if it is apparent that the slope of the $M_{\text{BH}}-\sigma_0$ relation is not well reproduced by the end-products of head-on accretion (empty circles). Note however that, while in the classical scenario the Magorrian relation is (obviously) nicely reproduced (Fig. 6), in case of substantial emission of gravitational waves the relation between BH mass and bulge mass is *not* reproduced (Fig. 6).

All the results presented in this Section holds under the strong assumption that the BHs of the merging galaxies are retained by the end-products, but there at least two basic mechanisms that could be effective in expelling the central BHs. The first is related to the general instability of three body systems: if a third galaxy is accreted by the end-product of a previous merging before the binary BH at its center merged in a single BH, then the escape of the smallest BH is highly possible. It is clear that if this process happens more than a few times, then the Magorrian relation will be not preserved at the end. A plausible solution to this problem is then to assume that the characteristic time of BH merging (first by dynamical friction on the background stars and then by emission of gravitational waves) is shorter than the characteristic time between two galaxy merging (for a

detailed discussion of this problem see, e.g., Milosavljevic & Merritt 2001, Yu 2002, Haehnelt & Kauffmann 2002, Volonteri, Haardt & Madau 2003). However, a second physical mechanism could be more effective in expelling the resulting BH from the center of a galaxy merger, i.e., anisotropic emission of gravitational waves. This process, commonly known as the “kick velocity”, is directly related to the fraction of BH mass emitted anisotropically during the BH coalescence (see, e.g., Flanagan & Hughes 1998, CvA). Gravitational waves in fact travel at the velocity of light, and so even the anisotropic emission of *a few thousandths* of the mass of the BH binary will produce a recoil (due to linear momentum conservation) of the resulting BH with a characteristic velocity higher than the escape velocity typical of massive galaxies. In conclusion, it seems to us not trivial to assume that in each galaxy merging the resulting BH will reside at the center (see, e.g., Haehnelt & Kauffmann 2000).

5 DISCUSSION AND CONCLUSIONS

As outlined in the Introduction, the present study is similar, in some aspects, to previous studies concerning the effects of merging on the FP. The results of our simulations are consistent with those of Capelato et al. (1995), based on N-body simulations of King (1966) galaxy models, and of Dantas et al. (2003), based on Hernquist models, who found that the edge-on FP is reproduced by dissipationless merging, owing to non-homology of the end-products. However, they considered only the first two or three steps of the merging hierarchy. In the same line of investigation, Gonzalez-Garcia & van Albada (2003) found that also the first generation of end-products of dissipationless merging based on Jaffe (1983) models preserves the FP when seen edge-on. At variance with these works, we used galaxy models with a substantially larger number of particles, we explored the cumulative effects of several generations of merging, and we also compared with other scaling laws, such as the Faber-Jackson, the Kormendy, and the $M_{\text{BH}}-\sigma_0$ relations.

The main results of our simulations can be summarized as follows:

- The edge-on FP is well reproduced by dissipationless hierarchical equal mass merging of one and two-component galaxy models, and by accretion simulations with substantial angular momentum, with their seed galaxies (i.e. the merging zeroth order generation) placed on the FP itself. On the contrary, in the case of head-on accretion, the k_3 coordinate *decreases* at increasing k_1 , at variance with real galaxies. The physical reason of these different behavior is due to a different evolution of structural non-homology of the end-products in the two scenarios; in fact the Sersic best fit parameter m grows monotonically with mass in equal mass mergers (and accretion with angular momentum), while *decreases* with mass in head-on accretion end-products.

- In both scenarios the scatter in the (k_1, k_3) coordinates associated to projection effects is of the order of the observed $1-\sigma$ dispersion of the edge-on FP.

- At variance with the results of the edge-on FP, all the results of our simulations are in qualitative agreement when plotted in the (k_1, k_2) plane, where the FP is seen nearly face-on. In this plane the mergers move parallel to the line

defining the zone of avoidance, and remain in the region of the FP populated by real galaxies.

- As a direct consequence of the numerical findings that the “observables” σ_0 and $\langle R \rangle_e$ follow closely the evolution of σ_V and r_V as predicted by the virial theorem, the end-products of our simulations fail to reproduce both the FJ and Kormendy relations. However, in the case of equal mass merging and accretion merging with angular momentum, the large values of $\langle R \rangle_e$ and the nearly constant values of σ_0 curiously compensate, and the end-products follow nicely the edge-on FP (see the first point above).

- Under the reasonable hypothesis that the derived values of σ_0 are not strongly affected by the dynamical evolution of binary BHs, our results show that dissipationless merging, while in accordance with the Magorrian relation, fails to reproduce the $M_{\text{BH}}-\sigma_0$ relation. We have then shown that, allowing for substantial emission of gravitational waves during the BHs coalescence, the $M_{\text{BH}}-\sigma_0$ relation is surprisingly reproduced, but the Magorrian relation is not. Merging by head-on accretion suffers of an additional problem when considered together with the Magorrian relation: our simulations in fact showed that the best Sersic m parameter decreases at increasing mass of the end-product, a behavior opposite to what is empirically found (Graham et al. 2001).

In conclusion the results of the presented simulations suggest that *substantial* dissipationless merging (especially when involving stellar systems of very different mass) cannot be the basic mechanism of formation of Es. We note, however, that our exploration of the parameter space is by no means complete, because in the simulations we did not consider initial conditions corresponding to *multiple* merging. In any case, indications exist that our results should be obtained also under these more general circumstances (Nipoti et al. 2003b). Finally, we note that from the numerical results one cannot exclude, on the basis of FP, FJ, and Kormendy relations, that Es could experience *few* occasional mergings with other Es, even in recent times as observed by van Dokkum et al. (1999). In any case, it is well known that many other astrophysical evidences, based on stellar population properties, such as the $M_{\text{g}_2}-\sigma_0$ and the color-magnitude relations, and the waveband dependence of the relation between mass-to-light ratio and galaxy luminosity (see, e.g., Pahre et al. 1998b, Pahre, de Carvalho & Djorgovski 1998a), strongly argue for a substantial dissipative phase in the formation of spheroids.

If we exclude dissipationless merging as the formation mechanism for Es, then we are left with two possible solutions, namely the monolithic scenario or a merging scenario where dissipation plays an important role. In this last case the presented simulations can also say something. In fact gas dissipation should be effective in shrinking the density distribution of the merging end-products, and, at the same time, increasing their central velocity dispersion, changes that are in the direction required by the FJ and Kormendy relations. In addition, in order to preserve the Magorrian relation, a fraction of the star forming dissipating gas must flow on the central BH, producing QSO activity; in this case the cosmological evolution of QSOs would be a tracer of the merging history, in accordance with the old ages of stars in Es. As a consequence, numerical simulations of galaxy merging in presence of gas (see, e.g., Bekki 1998), taking

also into account the feedback from the central BH in a self-consistent way (see, e.g., Tabor & Binney 1993, Binney & Tabor 1995, Ciotti & Ostriker 1997, 2001), and finally a better understanding of BH merging (see, e.g. Merritt & Ekers 2002; Hughes & Blandford 2002) are highly needed for a substantial progress in this field.

ACKNOWLEDGMENTS

L.C. would like to thank Giuseppe Bertin, Piero Madau, Jerry Ostriker, Silvia Pellegrini, Alvio Renzini and Tjeerd van Albada for useful discussions. We thank Reinaldo de Carvalho and the anonymous Referee for helpful comments. C.N. and P.L. are grateful to CINECA (Bologna) for assistance with the use of the Cray T3E and of the IBM Linux Cluster. This work was supported by MURST CoFin2000.

REFERENCES

- Athanassoula E., Fady E., Lambert J.C., Bosma A., 2000, MNRAS, 314, 475
- Barnes J.E., Hut P., 1986, Nature, 324, 446
- Bekki K., 1998, ApJ, 496, 713
- Bender R., Burstein D., Faber S. M., 1992, ApJ, 399, 462 (BBF)
- Bender R., Burstein D., Faber S. M., 1993, ApJ, 411, 153
- Bernardi M. et al., 2003, preprint (astro-ph/0301624)
- Bertin G., Ciotti L., Del Principe M., 2002, A&A, 386, 1491
- Binney J., Tabor G., 1995, MNRAS, 276, 663
- Bower R.G., Lucey, J.R., Ellis R.S., 1992, MNRAS, 254, 601
- Burstein D., Davies R.L., Dressler A., Faber S.M., Lynden-Bell D., 1988. In: *Towards understanding galaxies at large redshift; Proceedings of the Fifth Workshop of the Advanced School of Astronomy*, Dordrecht, Kluwer Academic Publishers.
- Caon N., Capaccioli M., D’Onofrio M., 1993, 265, 1013
- Capelato H.V., de Carvalho R.R., Carlberg R.G., 1995, ApJ, 451, 525
- Ciotti L., 1991, A&A, 249, 99
- Ciotti L., 1996, ApJ, 471, 68
- Ciotti L., 1999, ApJ, 520, 574
- Ciotti L., Bertin G., 1999, A&A, 352, 447
- Ciotti L., Ostriker J.P., 1997, ApJ, 487, L105
- Ciotti L., Ostriker J.P., 2001, ApJ, 551, 131
- Ciotti L., van Albada, T.S., 2001, ApJ, 552, L13 (CvA)
- Ciotti L., Lanzoni B., Renzini A., 1996, MNRAS, 282, 1
- Cole, S., Lacey, C.G., Baugh, C.M., Frenk, C.S., 2000, MNRAS, 319, 168
- Dantas C.C., Capelato H.V., Ribeiro A.L.B., de Carvalho R.R., 2003, preprint (astro-ph/0211251)
- Davies R.L., Efstathiou G., Fall S.M., Illingworth G., Schechter P.L., 1983, ApJ, 266, 41
- Dehnen W., 2000, ApJ, 536, L39
- Dehnen W., 2001, MNRAS, 324, 273
- Dehnen W., 2002, Journal of Computational Physics, 179, 27
- de Vaucouleurs G., 1948, Ann. d’Astroph., 11,247
- de Zeeuw T., 2001, in *Black Holes in Binaries and Galactic Nuclei*, Proceedings of the ESO Workshop held at Garching, Germany, 6-8 September 1999, ESO Astrophysics Symposia (Springer), 78
- Djorgovski S., Davis M., 1987, ApJ, 313, 59
- Dressler A., Lynden-Bell D., Burstein D., Davies R.L., Faber S.M., Terlevich R., Wegner G., 1987, ApJ, 313, 42
- Eggen O.J., Lynden-Bell D., Sandage A.R., 1962, ApJ, 136, 748
- Evstigneeva E.A., Reshetnikov V.P., Sotnikova N.Y., 2002, A&A, 381, 6

- Faber S.M., Jackson R.E., 1976, ApJ, 204, 668
 Ferrarese L., Merritt D., 2000, ApJ, 539, L9
 Flanagan E.E., Hughes S.A., 1998, PhRvD, 57, 4535
 Gebhardt K. et al., 2000, ApJ, 539, L13
 Gonzalez-Garcia A.C., van Albada T.S., 2003, submitted
 Graham A.W., Erwin P., Caon N., Trujillo I., 2001, ApJ, 563, L11
 Greengard L., Rokhlin V., 1987, Journal of Computational Physics, 73, 325
 Greengard L., Rokhlin V., 1997, Acta Numerica, 6, 229
 Haehnelt M.G., Kauffmann G., 2000, MNRAS, 318, L35
 Haehnelt M.G., Kauffmann G., 2002, MNRAS, 336, 61
 Hernquist L., 1990, ApJ, 356, 359
 Hughes S.A., Blandford R.D., 2002, astro-ph/0208484
 Jaffe W., 1983, MNRAS, 202, 995
 Jørgensen I., Franx M., Kjærgaard P., 1996, MNRAS, 280, 167
 Kauffmann G., 1996, MNRAS, 281, 487
 King I.R., 1966, AJ, 71, 64
 Kormendy J., 1977, ApJ, 218, 333
 Kormendy J., Richstone D., 1995, ARA&A, 33, 581
 Larson R.B., 1975, MNRAS, 173, 671
 Lauer T.R. et al. 2002, AJ, 124, 1975
 Londrillo P., Nipoti C., Ciotti L., 2003, preprint (astro-ph/0212130)
 Magorrian J. et al., 1998, AJ, 115, 2285
 Merritt D., 1996, AJ, 111, 2462
 Merritt D., Ekers R.D., 2002, Science, 297, 1310
 Merritt D., Ferrarese L., 2001, ApJ, 547, 140
 Milosavljevic M., Merritt D., 2001, ApJ, 563, 34
 Navarro J.F., Frenk C.S., White S.D.M., 1996, ApJ, 462, 563
 Nipoti C., Londrillo P., Ciotti L., 2002, MNRAS, 332, 901 (NLC02)
 Nipoti C., Londrillo P., Ciotti L., 2003a, in *The Mass of Galaxies at Low and High Redshift*, Proceedings of the ESO Workshop held in Venice, Italy, 24-26 October 2001, R. Bender and A. Renzini eds (Berlin: Springer), 70
 Nipoti C., Stiavelli M., Treu T., Ciotti L., Rosati P., 2003b, MNRAS, submitted
 Pahre M.A., de Carvalho R.R., Djorgovski S.G., 1998a, AJ, 116, 1606
 Pahre M.A., Djorgovski S.G., de Carvalho R.R., 1998b, AJ, 116, 1591
 Pentericci L., Ciotti L., Renzini, A., 1995, Astrophysical Letters and Communications, 33, 213
 Prugniel P., Simien F., 1997, A&A, 321, 111
 Sersic J.L., 1968, Atlas de galaxias australes. Observatorio Astronomico, Cordoba
 Spitzer L., 1969, ApJ, 158, L139
 Springel V., Yoshida N, White S.D.M., 2001, New Astronomy, 6, 79
 Tabor G., Binney J., 1993, MNRAS, 263, 323
 Tremaine S. et al. 2002, ApJ, 574, 740
 van der Marel, R.P., 1999, AJ, 117, 744
 van Dokkum P.G., Franx M., Fabricant D., Kelson D.D., Illingworth G.D., 1999, ApJ, 520, 95
 Volonteri M., Haardt F., Madau P., 2003, ApJ, 582, 559
 White S.D.M., Rees M.J., 1978, MNRAS, 183, 341
 Yu Q., 2002, MNRAS, 331, 953
 Ziegler B.L., Saglia R.P., Bender R., Belloni P., Greggio L., Seitz S., 1999, A&A, 346, 13